Ribagua
Revista Iberoamericana del Agua

ISSN: 2386-3781 (Print) 2529-8968 (Online) Journal homepage: http://www.tandfonline.com/loi/trib20

Rubble mound breakwater damage assessment through stereo photogrammetry in physical scale laboratory tests

Rute Lemos, João Alfredo Santos & Conceição Juana Fortes

To cite this article: Rute Lemos, João Alfredo Santos & Conceição Juana Fortes (2017): Rubble mound breakwater damage assessment through stereo photogrammetry in physical scale laboratory tests, Ribagua

To link to this article: http://dx.doi.org/10.1080/23863781.2017.1381455

Published online: 25 Oct 2017.

RIBAGUA, 2017
https://doi.org/10.1080/23863781.2017.1381455

Rubble mound breakwater damage assessment through stereo photogrammetry in physical scale laboratory tests

Rute Lemos[a], João Alfredo Santos[b] and Conceição Juana Fortes[a]

[a]Laboratório Nacional de Engenharia Civil; [b]Instituto Superior de Engenharia de Lisboa

ABSTRACT

Scale-model tests are usually required to evaluate the hydraulic and structural behavior of proposed rubble-mound breakwater designs. In order to speed up and ease the armor layer damage assessment, we developed a technique based on stereo photogrammetry. A key feature of this technique is its ability to compensate for the refraction in the air-water interface, thus producing a survey of the envelope of the armor layer without the need to empty the wave flume or wave basin where the scale model tests are carried out. This article describes this technique and the tests made to establish confidence in it and in the damage evaluation on a breakwater scale model. Results led to an error estimation of only fractions of a centimeter.

KEYWORDS

Breakwater; photogrammetry; rubble mound; scale model

PALABRAS CLAVE

Rompeolas; modelo físico; escala reducida; fotogrametria

Evaluación de daños de rompeolas de escollera con modelos físicos a escala reducida, a través de fotogrametría

RESUMEN

Los ensayos con modelos físicos a escala reducida son muchas veces necesarios, a fin de evaluar el comportamiento hidráulico y estructural del proyecto propuesto. Con el fin de acelerar y facilitar la evaluación de los daños a la envoltura del manto de rompeolas de la escollera, desarrollamos una técnica basada en la estéreo fotogrametría. La característica principal de esta técnica es su capacidad para compensar la refracción en la superficie entre aire-agua, produciendo así un levantamiento del manto resistente, sin necesidad de vaciar el canal o el tanque de oleaje donde los ensayos con modelos a escala se llevan a cabo. En este artículo se describe esta técnica y las pruebas realizadas para establecer una confianza en la evaluación de los daños con un modelo del rompeolas a escala reducida. El error resultó ser en fracciones de centímetro.

1. Introduction

Rubble-mound breakwaters are very interesting structures that create sheltered areas largely because of the simplicity of their construction (a quarry run landfill protected from sea-wave action by one or more layers of loose material of selected weight) and the ability to keep most of their functionality, even when some of the elements from the armor layer most exposed to sea-waves action are removed by incident sea waves. In fact, although this removal of armor layer elements means damage to the structure, it does not imply a total loss of its functionality because it can continue to protect the desired area almost completely, as the condition of the structure was restored as soon as the missing elements were replaced.

Until recently, the most common evaluation method for the condition of rubble-mound breakwaters (and of the consequent need for taking corrective interventions) was through the visual inspection of the emerged part (Santos et al., 2003). This method essentially identifies and counts the armor layer elements that have changed position since the last inspection, a procedure similar to the one used when studying the response of these structures to incident sea waves in scale-model tests. Also, aerial photographs have been used to assess changes on the armor layer of rubble-mound breakwaters. Hough and Phelp (1998) describe the procedures they use to compare the photographs taken during the inspection of rubble-mound breakwaters in South Africa and the information they get from it, which is essentially the motion of elements in the above-water part of the armor layer. Although such procedures can be applied in scale model tests, they don´t provide quantitative information for damage assessment concerning eroded areas and volumes.

CONTACT Rute Lemos rlemos@lnec.pt Laboratório Nacional de Engenharia Civil

With the increasing availability of means to survey the entire envelope of rubble-mound breakwaters (Silvestre et al., 2004) and to assess the maintenance needs of these structures along its life cycle, it makes sense to use a variable derived from these envelope measurements to quantify the damage such structures may suffer due to sea incidents therein.

The Hudson (1958) formula, the best known formula for the concept design of armor layer elements, determines the characteristic dimension of those elements to resist incident sea-waves with a given wave height, without any movements of those elements (i.e. without damage). Jackson (1968) investigated what happened to the armor layer elements when incident sea waves had a wave height greater than that contemplated in its design. To do so, damage was defined as the ratio of the volume of the armor layer elements displaced by the waves, by the total volume of armor layer elements in the tested breakwater stretch, something which implies the ability to identify and measure the volume of the displaced elements. A few years later, Van der Meer (1987) used a measure of the erosion of the cross-section of breakwaters built in deep water in the formula he presented for the concept design of rock armor elements. That formula resulted from scale-model tests, with the damage being defined as the ratio between the breakwater's cross-section eroded area and the square of a characteristic length of armor layer elements. The eroded area was obtained from the difference between the structure cross-sections surveyed at the beginning and at the end of the test with a mechanical profiler.

Wolters and Van Gent (2010), as well as Van Gent (2014) alone performed a set of physical model tests, in order to assess the effects of oblique waves on the stability of rock slopes and of cube-shaped armored rubble mound breakwaters (single and double layers). The damage to the armor layers was recorded by taking digital photographs before and after each test. For a number of tests with rock surveys of the armor layer envelope, there were also tests performed with a mechanical profiler.

Hofland et al. (2011) refers to the use of stereo-photogrammetry applied to rubble-mound breakwater surveys in scale model tests. Accuracy was estimated by comparison with a stretch of a sand bed, shaped to known dimensions, and by recording a scale model of a rock berm multiple times. The accuracy of the technique was better than 1 mm.

Nevertheless, if to carry out such surveys of the armor layer envelope, the wave flume or the wave tank where the scale model tests were carried out had to be emptied, it would be a time-consuming task.

Ferreira et al. (2005) proposed a method for the reconstruction of submerged scenes from image pairs, by using a procedure which is essentially similar to the one used in close-range photogrammetry or stereo photogrammetry. Such a procedure enables the survey of the armor layer envelope and avoids the downtime associated with emptying the wave flume or the wave tank.

This paper aims to systematize the experience that has been gained in the use of the Ferreira et al. (2005) technique, and to show that by using common cameras, i.e. with a low budget, you can survey the emerged and submerged part of rubble-mound breakwaters and assess the damage through scale models of these structures. After this introduction, there is a description of the evaluation of armor damage in scale model tests of rubble-mound breakwaters. The method of Ferreira et al. (2006) is presented in chapter 3, whereas the tests made to assess the errors in the measurements with this technique, as well as the influence of the water column height in those errors, are presented in chapter 4. This chapter also includes the procedures used to assess damage evolution in such surveys. The paper ends with the conclusions and recommendations on the use of this survey method.

2. Damage assessement in scale models tests of rubble-mound breakwaters

Breakwaters are built to reduce wave action in an area to the lee of the structure. Wave action becomes reduced through a combination of reflection and dissipation of incoming wave energy.

When used for ports, breakwaters are constructed to create sufficiently calm waters for safe mooring and loading operations, handling of ships, and protection of harbor facilities.

Rubble-mound breakwaters are the most commonly applied type of breakwater. The conventional rubble-mound structures consist of a core of finer material covered by large blocks forming the so-called armor layer. To prevent finer material from being washed out through the armor layer, filter layers must be provided. The filter layer just beneath the armor layer is also called the underlayer (CEM, 2006 a).

A rubble-mound breakwater may also have a concrete superstructure that serves several purposes, for example: providing access for vehicles, including cranes for maintenance and repair, and accommodation of installations such as pipelines.

Figure 1 shows a cross-section with two examples of rubble-mound breakwaters. Concrete armor units are used as armor blocks in areas with rough wave climates or at sites where a sufficient supply of large quarry stones is not available.

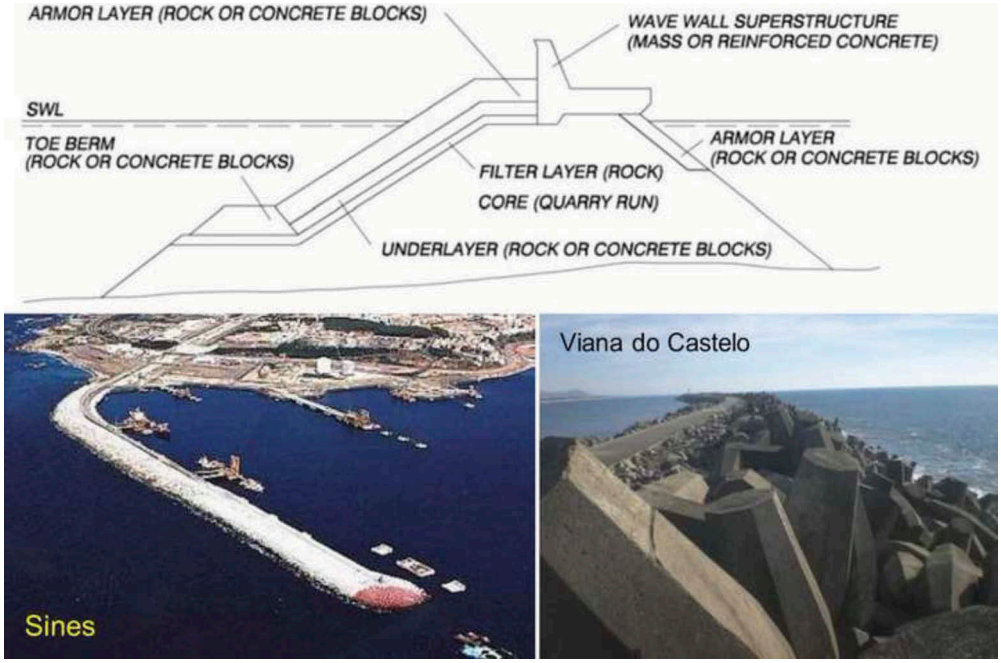

Figure 1. Rubble-mound breakwaters at Sines and Viana do Castelo harbours (Portugal).

The concept design of armor layer elements always has to be fine-tuned with scale model tests. In fact, in spite of the formulae used in such a concept design being obtained from scale model tests, they were established for a limited set of parameters both for incident sea waves and armor layered geometry.

In the scale model tests, the span of the structure to be studied is scaled down to be built at a wave flume or wave tank, which is then exploited according to Froude similarity law. This means that the flow-induced forces associated with the sea-waves generated from the model to check or to fine tune the concept design do obey the Froude similarity law, the length scale being imposed by the scale at which the structure's stretch was built in the wave flume or wave tank. This implies having a scale for the significant wave heights and another for the peak periods of the sea states generated in the tests with the scale model.

Such scale model tests aim at characterizing the structure's response to incident sea waves in terms of overtopping (the average volume of water that flows over the structure's crest, that was being evaluated then), or in terms of armor layer damage. Based on such results, changes could be adopted in the crest level, in the armor layer slope, or in the weight of the armor layer elements.

Damage to armor layers is characterized either by counting the number of displaced units or by measuring the eroded surface profile of the armored slope. In both cases, damage is related to a specific sea state of a given duration.

When damage is characterized in terms of displaced units, it is usually given as the relative displacement, *D* (the ratio of displaced units to the total number of units, or preferably, to the number of units within a specific zone around the still water level.

In fact, structures with the same geometry and armor-layered units that are subjected to the same incident sea states (significant wave height and peak period or wavelength) are expected to have a similar number of displaced units, but they would have different relative displacements if they have different lengths of the respective armored slopes.

Damage can be related to any definition of armored layer movements, including rocking. The relative number of moving units can also be obtained with the total number of units within a strip of width D_n stretching along the slope from the bottom to the top of the armored layer (Figure 2). For this strip displacement definition, van der Meer (1988) used the term N_{od} for units displaced out of the armored layer and N_{or} for the rocking units. The disadvantage of N_{od} and N_{or} is, again, their dependence on the slope (strip) length.

Because almost all armor unit movements take place within the strip comprised between still water level ± Hs, the number of armor units within this reference area is adopted to calculate *D*. Since the width of such a strip (and consequently the number of armored units there) changes with Hs, it is recommended to use the

Figure 2. Slope division into strips of width D_n.

number of units within the region defined by the still water level ± *n* x D_n, where:

- D_n is the nominal diameter;
- *n* is chosen such that almost all movements take place within these levels (CEM, 2006 b).

Damage characterization based on the eroded cross-section area A_e around the stillwater level was used by Iribarren (1938) and Hudson (1958). Hudson defined *D* as the percent erosion of original volume. Iribarren defined the limit of severe damage that could occur when the erosion depth (de) in the main armored layer reached the nominal diameter of the armor layer elements (D_n).

Broderick and Ahrens (1982) and Van der Meer (1988) defined a dimensionless damage parameter, given by Equation 1:

$$S = \frac{A_e}{D_n^2} \qquad \text{(Eq.1)}$$

where A_e is the eroded cross-section area around the still water level (Figure 3) and D_n the nominal diameter of the armored units. Thus, S is a dimensionless damage parameter, independent of slope length.

Figure 3 presents another quantity that may be used to characterize the damage in a cross-section of the armor layer of a rubble-mound breakwater, namely, the eroded length L_e, which is the distance measured along the idealized design slope between the extremities of the eroded area.

Although the value of the dimensionless damage parameter is obtained in each of the cross-sections considered in the studied breakwater stretch, one must compute the average of the values obtained in cross-sections where they are non-zero or above a preset threshold, to obtain the characteristic value in the

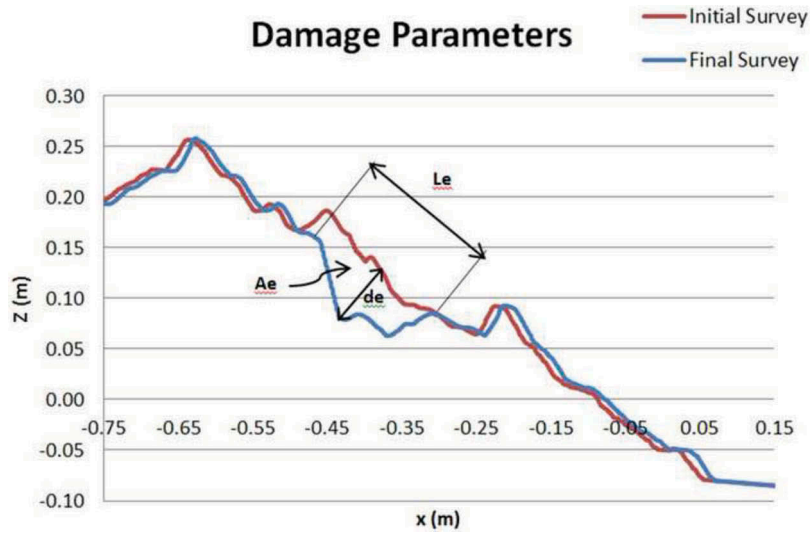

Figure 3. Breakwater slope damage parameters A_e (eroded Area), L_e (eroded length), and d_e (eroded depth).

mentioned stretch. For eroded length or eroded depth, the determination of the corresponding characteristic values is very easy, since one may have to find only their maximum values in the studied stretch.

From the previous explanation, one may conclude that the quantities of interest to measure in the scale model tests are the number of armor layer elements that were displaced from their initial position in the armored layer (of relevance when damage is computed as the fraction of displaced armor layer elements) and the z coordinate of points on the armored layer envelope before and after the tests – from which one can evaluate the eroded volume, the maximum erosion depth and the maximum length of the eroded area along the armor layered slope. It is planned to use the same procedures to characterize the prototype damage, as the most reasonable quantity to evaluate in the prototype is the z coordinate of points on the armored layer envelope, because it can be obtained from surveys of that envelope that can be carried out at fixed time intervals or after the occurrence of important storms. The number of displaced armor layer elements may be easily assessed in the prototype when the rubble-mound breakwater is built in a large tidal range area, especially the armored layer elements in the slope region above the low spring tide.

3. Methods: Stero-photogrammetry

Stereo photogrammetry is based on the same principle of binocular vision, where the image that is individually captured by each eye is transmitted to the brain, which merges both images. These are slightly different from one another, due to the perspective from each eye, allowing creation of a 3D representation of the observed scene, resulting in the so-called stereo vision or stereopsis.

A stereo photogrammetry system needs two images (usually called the right and left image) of the same scene, taken from different perspectives.

To simplify the method and the computation procedures associated to camera calibration and image correction, it is common to have cameras with parallel axes. Such an approach makes the process simple, because there is just one translation between the left and right images and no rotation has to be taken into account (Figure 4). Since the left and the right images are slightly different due to the distance *b* between both cameras, both those cameras have a different view of the same real-world point *P*. Through stereo matching, one may get the so-called "disparity" for each common point in both images, which is the difference between the *x* coordinates of the same point in both images (Lagendijk, Franich & Hendriks, 2002).

The key point here is the correspondence between the pixels in the right and left images, implying the need for the so-called image rectification process, where possible radial and tangential distortions created by the camera ocular system are corrected. Corresponding points between the two images must satisfy the so-called epipolar constraint (Loop and Zang, 1999), which will reduce the search space for corresponding points to a 1-dimensional line; however, to make such a rectification possible, a previous calibration of the cameras is needed. The calibration process enables the definition of the intrinsic parameters of the two cameras (focal distance, image center, lens distortion parameters), as well as the extrinsic parameters (metric used to measure distances and angles, as well as the absolute position of the three-dimensional reconstructed scene).

The intrinsic parameters enable the conversion between the pixel units and the units used to measure

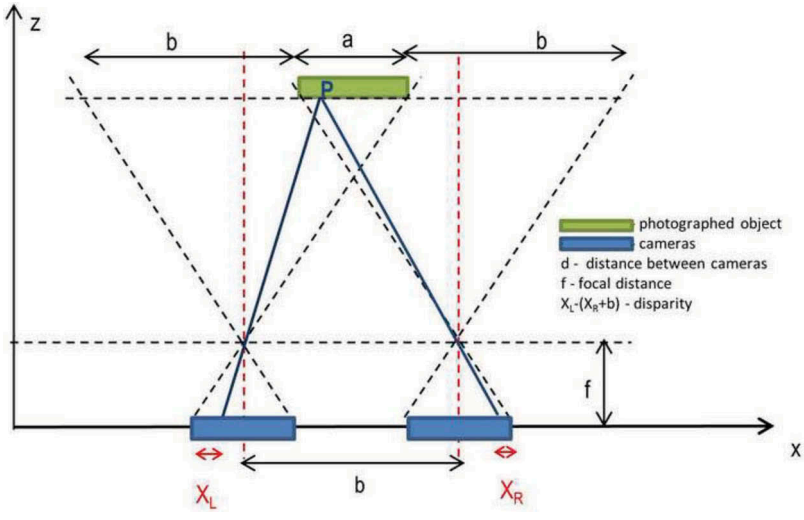

Figure 4. Camera setup using parallel axes.

the 3D scene, and the extrinsic parameters define the relative position of each camera (by position and orientation) with relation to a point in space. Both parameters are obtained in the camera calibration, which uses a procedure based on the work of Zang (1999): several image pairs from a chequered board of known dimensions are obtained and in those images, the manual identification of notable points is made. When clicking the corners in the images, one corner can be picked to define the origin of the world referential (Figure 5). Usually, 15 image pairs are enough to get the cameras' intrinsic parameters. For the extrinsic parameters one image pair of the same target now placed on $z = 0$ plan is enough.

A pairing or correspondence procedure attributes to a point in one of the images, its correspondent in the other. In our case, use is made of the Sun (2002) algorithm, which is deemed adequate to dense stereo reconstruction, as would happen in our problems.

The disparity map indicates, for each pixel, the difference between its location in the left and right image. Based on such a map, if the focal distance (f) and the distance between the camera axis (b) and the x coordinate of the point in both images (x_L and x_R) are known, it is possible to determine the depth of a point that appears in both images (Mattoccia, 2015).

Knowing the depth of each point that appears in both images, it is possible to make the 3D reconstruction of that scene.

As can be seen in Eq. 2, one of the key parameters in depth determination is the distance between the cameras. It can be shown that as such distance decreases, the superposition between the left and the right images increases (Figure 4).

$$Z = f + \frac{f \cdot b}{X_L - (X_R + b)} \qquad \text{(Eq.2)}$$

The error in the depth evaluation decreases as the distance between the cameras increases; however, that means the distance between the cameras should be as large as possible, so as to reduce the error in depth evaluation, without preventing the correlation between homologous points in the image pairs.

The standard procedure for reconstruction of emerged scenes was modified by Ferreira et al. (2005) and Ferreira (2006), to deal with images from a completely submerged scene. The main difficulty here is that the known epipolar constraint, which helps reduce the search for a match, is not usable because of the fact that straight lines underwater do not project as straight lines in an image, due to the refraction of light rays on the air-water interface. Then, for each pixel within one image, it's possible that the matches are along a curve that is different for every point on the object. Essentially, this means that most stereo algorithms are not usable.

Ferreira et al. (2005) showed that, if the incidence angle is small (below 20 degrees), the linear part of the Taylor Series expansion, which is equivalent to modifying camera parameters, is precise enough for our purpose. In other words, current stereo algorithms can be used if the camera orientation parameters are within a certain range.

In fact, the non-linear relationship between the light ray emitted from a point above the interface and its refracted ray can be simplified by expanding it in a Taylor series and retaining the first-order terms. When the incidence angle is below 20 degrees, using the Taylor approximation for the refraction angle implies an error smaller than 0.5 degrees with relation to the real refraction angle. This approximation leads to simple rectification processes cancelling most of the distortion introduced by the interface. It can be shown that all light rays converge at a single point p1, as is illustrated in Figure 6. The path of various light beams are drawn and bent by the interface. If these bent light rays are extended back to the original media, they all converge at a point, allowing for a virtual camera to be placed at that location.

This fact hints at the possibility of rectifying the image with refraction effects, by only changing the extrinsic camera parameters. In other words, by approximating Snell's law, the problem with refraction

Figure 5. Example of a stereo pair and calibration board, used to calibrate the camera setup.

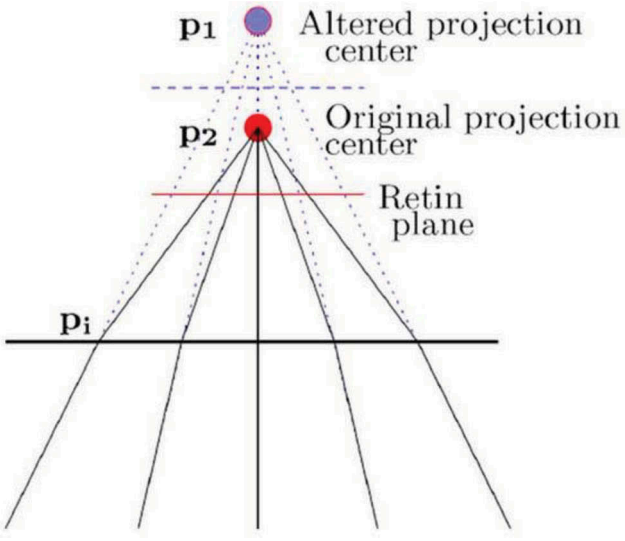

Figure 6. First order approximation of Snell's law (Ferreira, 2006).

is transformed into a typical stereo problem without the air-water interface. All that remains to be done is to project the original image onto the $z = 0$ plane and to project it back to a virtual camera with projection centre at p_1.

Despite the complexity of such procedures, this method has the great advantage of allowing the realization of the survey of the scale model envelope without the need to empty the wave flume or the wave tank where the model was built.

In brief, the major steps of this method are:

(1) Calibration of each camera's intrinsic parameters. This step also includes a preliminary image rectification, to eliminate the radial and tangential distortion introduced by the ocular system of each camera.
(2) Calibration of the extrinsic parameters that are of paramount importance for the triangulation, as they define the relative position and orientation of each camera with relation to a point in space. Calibration of these parameters and of the intrinsic parameters usually contributes toward reducing the search space in the correspondence problem.
(3) Correspondence, which is attributed to a point in one of the images, with its correspondent in the other. This step is often the most difficult and the most prone to errors, although there are restrictions and transformations that can be applied to images, greatly simplifying the problem.
(4) Conversion of previous results into 3D data. This conversion is usually simple, and with properly rectified images, it boils down to a projective transformation.

The final product of this process is a file with the coordinates of the pixels that are common to the right and left images. Although the pixels used in the reconstruction of the observed scene are evenly distributed in the image, this does not imply that the corresponding points are equally spaced along the y or x coordinates. As seen in the next chapter, the spacing change is not significant; however, to facilitate the comparison between successive surveys or to get an envelope profile along any direction, it is usual to adjust a surface to the cloud of points of the reconstructed scene. Such a surface is defined at a regularly spaced grid (along the x and y axes), the result of joining the triangular surfaces created from adjacent points of that cloud, with the z coordinate of the grid points being obtained by linear interpolation of the z coordinates of the defining points of those triangular surfaces. Figure 7 illustrates the 3D reconstruction of a partially submerged physical scale model of a breakwater.

4. Results and discussion

The stereo photogrammetric survey technique introduced by Ferreira et al. (2005) was first tested in long-term scale models for two and three dimensional scale models, where Antifer cubes or rocks were used (Afonso, 2008; Lemos, 2010). Several tests were also carried out, aiming to measure the breakwater armor layer erosion, in which both natural and artificial units were used (Lemos and Santos 2012). Although those tests showed the potential for this technique, it was not quantified with the survey technique's reliability and precision.

All the tests shown below were obtained using photographic equipment that consisted of: two cameras mounted side by side, in a support structure set 2.0 m above the air-water interface and able to photograph simultaneously the same scene. The camera separation baseline was of 0.16 m (Figure 8). In all the tests, we used a focal length of 35 mm and an aperture of f/9 adjustment.

Throughout the tests herein described, two digital SLR cameras (Canon EOS 350D) fitted with fixed focal length lenses (Canon EF 35mm $f/2$) were used. This setup is capable of acquiring images with 3456 by 2304 pixels (8.0 megapixel), as well as images with 2496 by 1664 pixels (4.1 megapixels) and 1728 by 1152 pixels (2.0 megapixels).

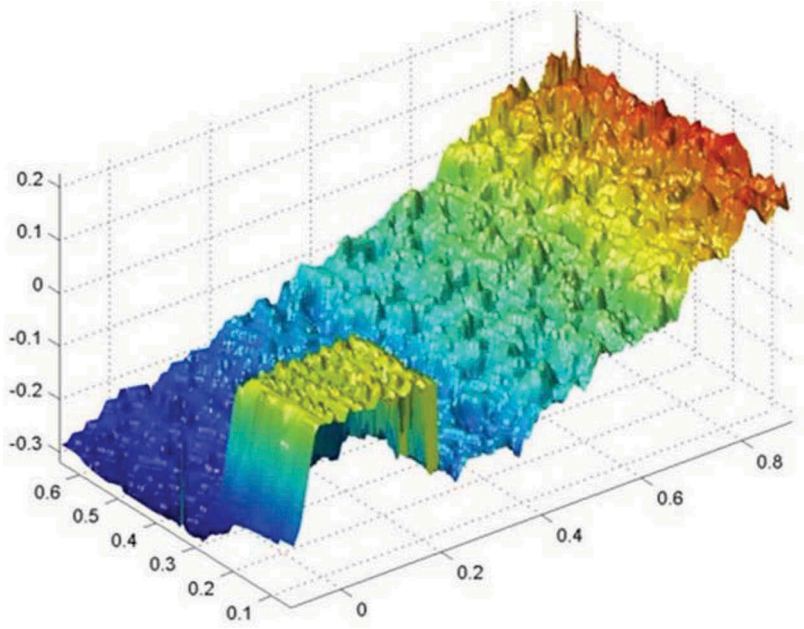

Figure 7. Three-dimensional (3D) representation of a physical scale model of a rubble-mound breakwater.

Figure 8. Camera layout above the wave flume.

4.1 Accuracy evaluation

The first verification exercise of the Ferreira et al. (2005) procedure consisted of surveying a smooth slope created by a board placed in a flume, to overcome a vertical drop of 0.31 m on a length of 0.69 m along the flume (Figure 9). The water depth in the flume in front of the model was about 0.18 m, thus about one half emerged and the other half submerged.

The image resolution used for the breakwater model survey was of 2496 by 1664 pixels. The computing time of the stereo photogrammetric reconstruction of the envelope survey was about a minute, using an Intel Core i7 computer at 2.93GHz.The reconstruction x coordinate spacing has an average of 0.00056 m with a standard deviation of 0.00008 m, whereas the reconstruction y coordinate spacing has an average of 0.00067 m, with a standard deviation of 0.00037 m.

By taking a cross section approximately at the middle of the board width (0.30 m), which corresponds to a pixel column that is 118 pixels away from the right edge of the reconstructed scene, one gets the profile represented in Figure 9. In figure 9 one can see that the reconstructed scene does not have a continuous variation in the z coordinate; so, instead of a smooth profile

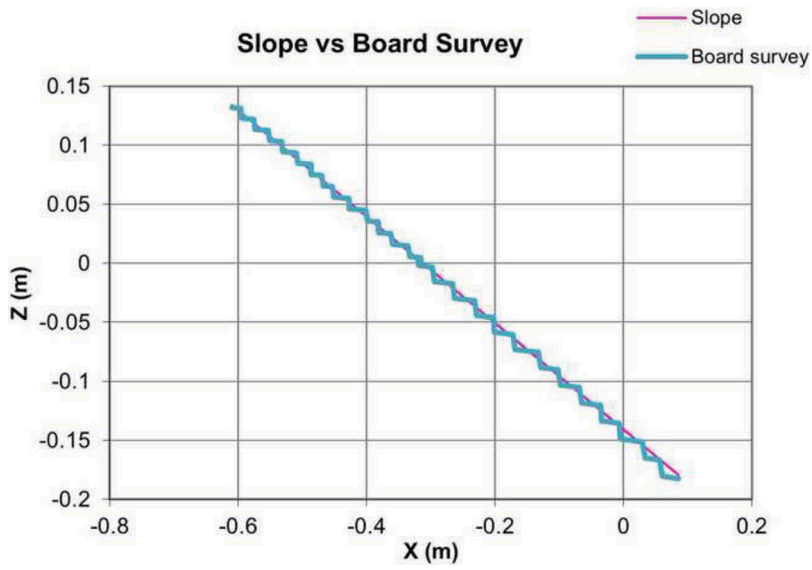

Figure 9. Slope versus surveyed board representation.

one gets a jagged one. This may be due to problems with the identification of chromatic differences between pixels in the same image with difficult depth evaluation.

In analyzing the y coordinate values corresponding to this cross section, it is clear that choosing a pixel column of the reconstructed scene matrix does not imply a constant y value.

A statistical analysis shows that the minimum y value is 0.35 m and the maximum is 0.355 m, the average being 0.352488 m and the standard deviation 0.001442 m. These numbers show that the variation in the y values for this profile is not very important.

Figure 10 presents the evolution with z of the error in the scene reconstruction of the sloping board, i.e. the absolute value of the difference between the z coordinates in the profile and in the sloping board. The raw data column in Table 1 presents the maximum error per 5 cm high interval, the maximum value. It is clear both in this table and in the figure that the error is more important in the submerged part of the sloping board, and that it increases as the height of the water column above the surveyed point increases.

A procedure to smooth the raw profile obtained directly from the cloud of points consisted in applying a centered moving average. The errors obtained with such a moving average of the z coordinate of 5, 11, 21 and 31 contiguous points are presented in Figure 10, whereas a detail of the surveyed profile, using the different smoothing types, is presented in Figure 11.

The maximum errors in the 5-cm high intervals resulted from that smoothing are presented in the corresponding columns of Table 1. The trend in error increases observed for the raw profile is again evident in the smoothed profiles.

One may conclude that the maximum error obtained at the deepest part of the sloping board with the moving average of the z coordinate of 21 contiguous points, 0.0087 m, is quite acceptable and so such a moving average can be recommended for profiles obtained directly from the cloud of surveyed points.

There is one last profile presented in Figure 10 and in Figure 11, obtained from the surface being defined by regularly spacing in the x direction (0.03 m) and in the y direction (0.03 m) using linear interpolation in the cloud of points of the reconstructed scene. The maximum error associated to this profile is presented in the Table 1 column "Grid with interpolation"; however, this profile keeps the jagged aspect of the raw profile and does not coincide with it. This may be due to the fact that the regularly spaced grid points do not coincide with cloud points. Anyway, the error does not change much with the z coordinate and it is comparable with the error in the previously-mentioned smoothed surveys.

A second test of the accuracy of the surveys obtained from submerged scene reconstruction was carried out by comparing the two surveys obtained at the end of a model test, one of them obtained before emptying the wave flume and the other one with no water in the wave flume. Figure 12 is a scale model of a rubble-mound breakwater that was exposed to wave action and was partially damaged. The armored layer had an initial slope of 1:2 and was made of rock with a

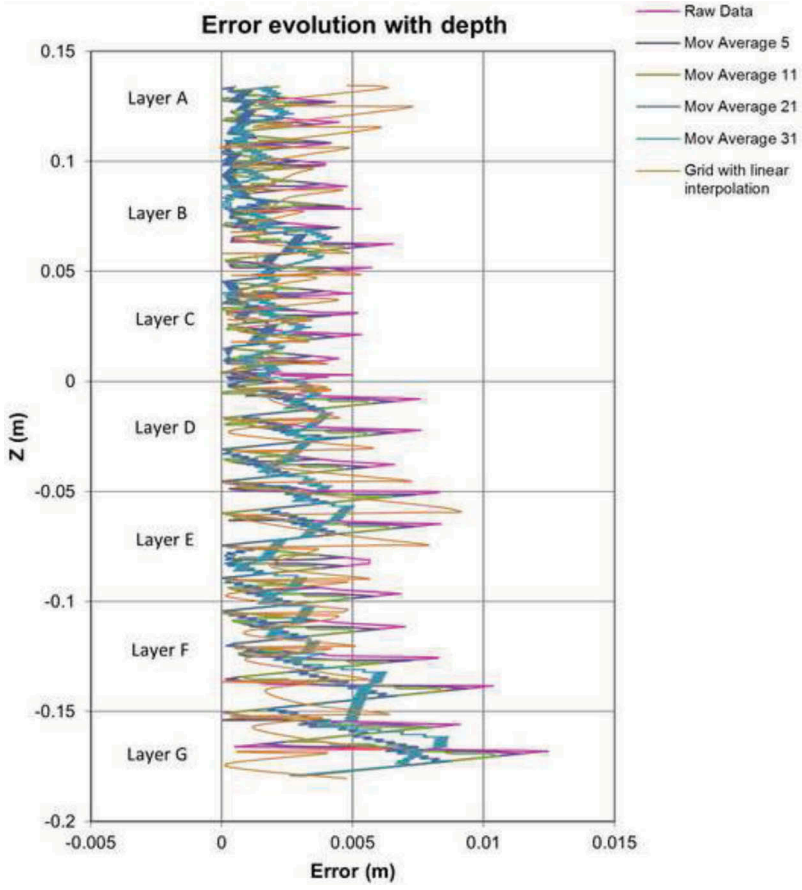

Figure 10. Error evolution with depth, in the scene reconstruction of the sloping board.

Table 1. Maximum error per layer (m).

Layer	Raw Data	Moving Average 31	Moving Average 21	Moving Average 11	Moving Average 5	Grid with interpolation
A	0.0045	0.0017	0.0013	0.0033	0.0042	0.0073
B	0.0065	0.0031	0.0033	0.0047	0.0055	0.0048
C	0.0053	0.0023	0.0022	0.0039	0.0047	0.0052
D	0.0082	0.0032	0.0047	0.0057	0.0066	0.0071
E	0.0084	0.0040	0.0047	0.0065	0.0074	0.0092
F	0.0104	0.0052	0.0067	0.0085	0.0094	0.0056
G	0.0124	0.0075	0.0087	0.0106	0.0114	0.0063

nominal diameter of 36 mm. The structure height was of 0.31 m and the water depth in front of the structure toe was 0.158 m, which means that about 50% of the slope was submerged.

The cross-sections, obtained in the central region of the model for the two conditions, are shown in Figure 13, as well as the evolution with the z coordinate of the difference between the two profiles, taking as a reference the survey without water in the wave flume.

Figure 13 signals the maximum error in each of the 5-cm depth sections that can be defined in the profile.The image resolution used for the breakwater model survey was of 2496 by 1664 pixels. The computing time of the stereo photogrammetric reconstruction of the envelope survey was about a minute, using an Intel Core i7 computer at 2.93GHz.

The reconstruction of the x coordinate spacing had an average of 0.00078 m with a standard deviation of 0.00057 m, whereas the reconstruction y coordinate spacing was an average of 0.00060 m with a standard deviation of 0.00031 m.These profiles were extracted from the surfaces defined by a regularly spaced grid (0.03 m in the x direction and 0.03 m in the y direction) by linear interpolation of the points in the cloud of the reconstructed scenes.

Unlike what happened with the sloping board, the error does not increase with the water depth. In fact, larger errors were obtained at the emerged part of the slope, where the coincidence of both surveys was expected. This could be due to changes in the light between the photos taken with and without water in the flume. Both surveys also show that increasing the chromatic differences in the photographed scene contributes to a successful survey with the photogrammetric

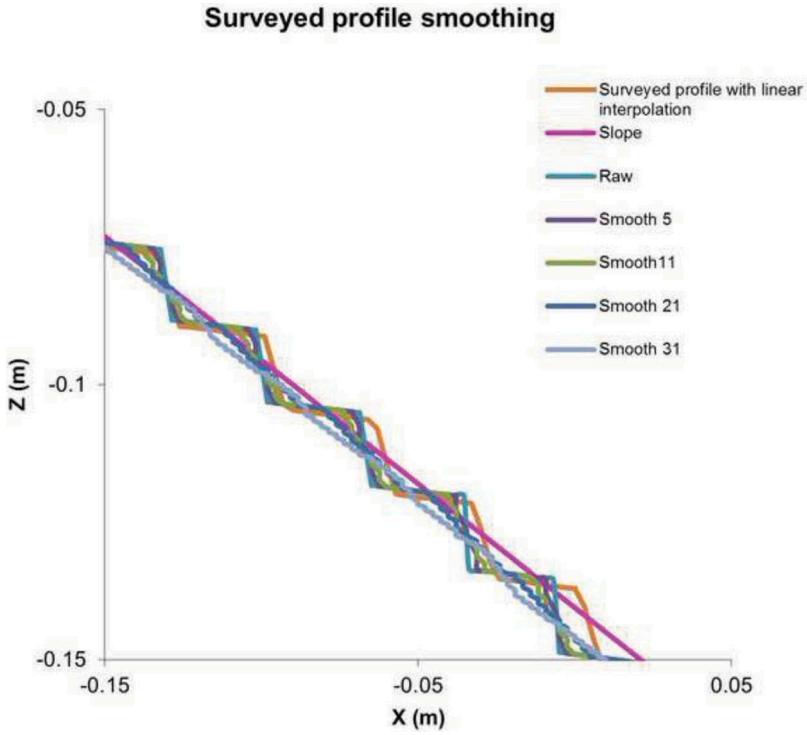

Figure 11. Detail of the profile survey, using different smoothing types.

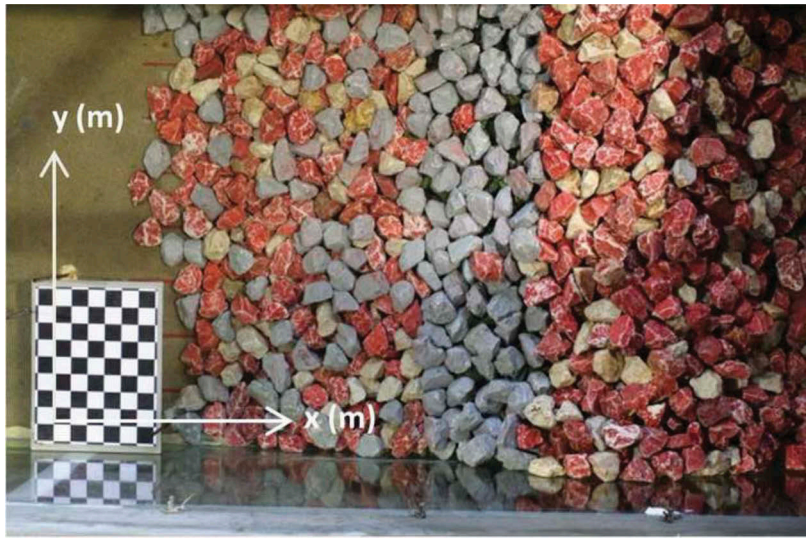

Figure 12. Profile survey of the scale model.

technique. Colored rock elements provided better chromatic differences and a more texturized image than the monochromatic sloping board, which can explain the absence of *z* coordinate clustering in this second test case.

4.2 Damage evolution

The last exercise was the assessment of the damage evolution from the surveys based on scene reconstruction. The evaluation of the maximum erosion area (A_e), erosion length (L_e) and erosion depth (d_e) was made using a simple program that uses the following sequence of procedures:

- Introduction of the original slope alignment that will serve to define the orientation of the new reference system (X0Z in Figure 14).
- Transform coordinates of the defining points of the profiles to the new reference system. All

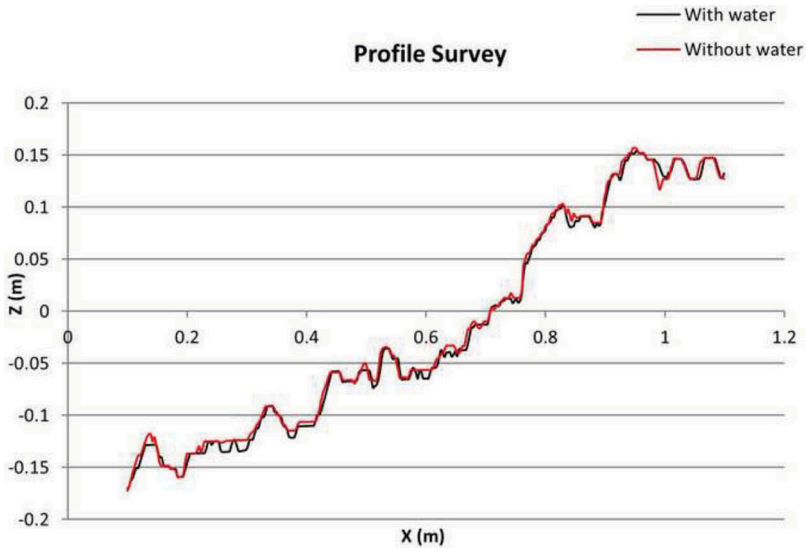

Figure 13. Cross-sections obtained from the surveys conducted with and without water in the flume.

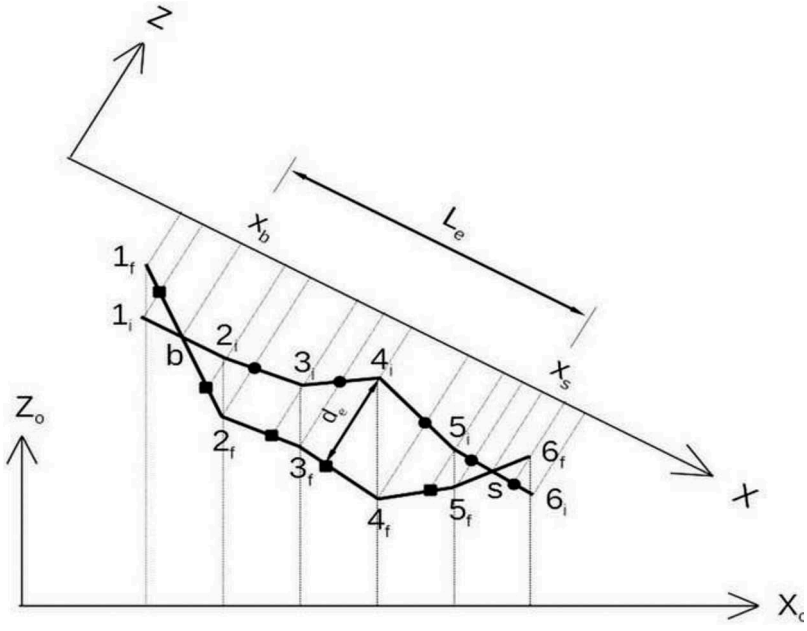

Figure 14. Outline of the procedures to compute L_e, d_e and A_e.

statements below relate to coordinates in the new reference system.

- As the new abscissa of those points no longer coincide, create a list of all the different abscissae and calculate, for the initial profile (index i in Figure 14 and the final profile (index f in the same figure), the corresponding ordinates for those abscissae. This means that new points do appear in the profiles (marked by circles in the initial profile and marked with squares in the final profile of Figure 14).
- Sweep the two profiles in the positive direction of the abscissa, looking for changes in the sign of the difference between the ordinates of points on the final and initial profile with the same abscissa. When such change occurs and the ordinate difference between the following points is negative, the beginning of an area where erosion of the initial profile occurred is found (point b of abscissa xb between x1i and x2i in Figure 14).
- While not another change in the sign of that difference occurs, one is in the same erosion

zone. This implies the total eroded area is increased with the eroded area between consecutive points of both profiles, and that the maximum depth of that erosion zone is updated with the ordinate difference between the two profiles.

- Once the end of the erosion zone is reached, the difference between the abscissa of the stopping point and beginning point ($x_s - x_b$) defines the length of the erosion zone (L_e in Figure 14). In addition, the area of the erosion zone (A_e) and the maximum eroded depth of the same zone (d_e in the same figure) are defined.

When the sweeping of the profile is complete, the largest erosion area and the corresponding maximum depth are selected.

We carried out tests with a scale model of a rubble-mound breakwater whose armor layer had a slope of 3:2, and was made of rock with a median diameter of 40 mm, where 130 colored tetrapod units were scattered in a 0.33 m^2 area, in order to provide some chromatic differences. Stereo pairs were obtained at the undamaged profile and at two stages of growth of a hole that was made in the armored layer, by manually removing armor layer elements. In this case, all the images were obtained with almost no water in the wave flume. The model height was of 0.30 m.

Figure 15 a shows the final stage of the hole, whereas Figure 15 b presents the profiles obtained at three different growth stages: I – the initial profile; II – after removing seven tetrapods (three of them were contained on the represented section); and III – after removing 12 rocks (five of them contained on the represented section). By comparing the eroded area (0.0085 m^2) with the characteristic area of the removed armor units - $(Dn_{50})^2$ = 0.0016 m^2, it corresponds approximately to the area of the removed tetrapods, plus empty spaces.

Table 2 summarizes the damage parameters corresponding to these three stages.

4.3 Discussion

Experience can tell that any survey method of submerged surfaces scenes in scale model tests using photogrammetric methods is a very time-consuming

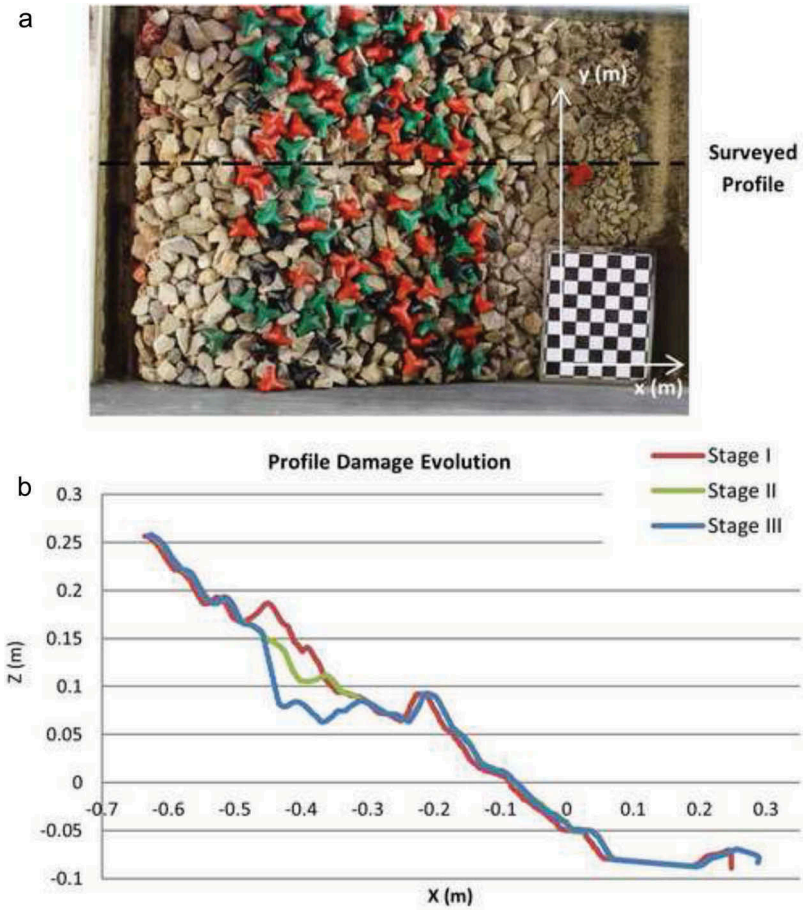

Figure 15. a) Damaged armor layer; b) Profile damage evolution.

Table 2. Damage parameters corresponding to stages I to III.

	Le (m)	de (m)	Ae (m^2)
Stage I	0	0	0
Stage II	0.159	0.0972	0.0042
Stage III	0.267	0.147	0.0085

task, especially if the channel or basin needs to be drained; however, the measurement of the eroded volume can be carried out using a technique based upon the reconstruction of stereo pairs, where refraction due to the air water interface is corrected, avoiding having to empty the flume or tank.

Ferreira (2006) show that in their experience, the quality of the reconstruction begins to degrade for incidence angles greater than 15 degrees, for a conventional stereo setup. To test the viability of the Snell correction, the Persistence of Vision Raytracer (POV-Ray) to generate a few synthetic images of a submerged plane parallel to the interface at various depths. The cameras were positioned at 1.3 m above the interface, with a baseline of about 0.3 m. The reconstruction algorithm with correction of the refraction on the interface led to a maximum error on the overall image was of 3 cm at a depth of 1.5 m. This results in a relative error in depth estimation of about 2%.

In the present work, the accuracy of the technique was tested on real images taken from a smooth slope created by a board and an armor layer consisting on rock units with a nominal diameter of 0.036 m. Tests were performed with cameras positioned 2.0 m above the interface, a baseline of 0.16 m and a focal length of 35 mm and an aperture of f/9 adjustment.

The accuracy at a depth of 0.3 m was of 0.0124 m with raw data and 0.0087 m with a moving average smoothing of 21 points. This error corresponds to less than half the nominal diameter, and considering that model dimensions used in the present tests were 1:30 and 1:40, the maximum survey error in the prototype would be around 0.3–0.4 m.

The main advantage of this method is to enable good results, with the accuracy necessary for measuring armor layer erosion in the scale model tests making use of cost-effective, good resolution, commercial off-the-shelf, digital cameras.

5. Conclusions

In this paper, a stereo photogrammetric method for making a profile survey was described. Two-dimensional accuracy and damage measurement tests were conducted in order to tune the technique, as well as to speed up the data post-processing.

The accuracy tests aimed to test the survey precision by:

- Evaluating the error progression with the depth by using a sloping, monochromatic, half-submerged pad. This test showed that the error increases with the water depth and that the surveyed profile resulted in a jagged cross-sectional representation;
- Evaluating the error progression when applying a moving average of 5, 11 and 21 points; and also a grid with linear interpolation in order to avoid a jagged survey profile. The moving average of 21 points showed the best relation error/profile smoothing, enabling to process raw data from the cloud of points;
- Evaluating the error progression with the depth, using a real scale model of a breakwater (i.e., an observed scene with more chromatic differences). This evaluation was achieved by comparing two surveys obtained at the end of a model test, one before emptying the wave flume and the other with no water in the wave flume. In this case, the profiles were obtained from a surface defined on a regularly spaced grid.
  From the results, one may conclude that the error does not vary much with the depth and its average was of 0.004 m. The maximum error, 0.022 m, was obtained at a single zone in the emerged part of the slope, where the coincidence of both surveys was expected. This was probably caused by a stereo matching problem.

After establishing the confidence in the technique capability of surveying submerged scenes, a damage assessment test was conducted, aiming to assess damage evolution by using a simple program, whose output was the maximum erosion area, the erosion length and the erosion depth. These final test results were consistent with the model dimensions.

As a final conclusion, this work suggests that the stereo photogrammetric technique:

- It is of simple use. Nevertheless, the camera calibration procedure should be carefully carried out, because all the following procedures depend on it;
- Produces reliable surveys, even with submerged scenes with an error that may be considered negligible;
- Is a cost-effective technique, as it requires only two photographic cameras. They provide useful information: eroded area, eroded depth, eroded

length and other geometrical information from the cloud of points of the reconstructed scene;
- Data post-processing is simple, taking about one minute to get the scene reconstructed, and about two minutes to process the resulting cloud of points. To define a surface or extract a profile is a matter of seconds;
- Different color pattern arrangements of the armored layer blocks lead to a better photogrammetric reconstruction.

References

Afonso, C. (2008). *Influência da Obliquidade da Agitação e da Densidade de Colocação dos Blocos Antifer na Estabilidade de Obras Marítimas de Talude*. Master degree thesis, Instituto Superior Técnico, Lisbon, Portugal

Broderick, L. E. and Ahrens, J. P. (1982). *Rip-rap stability scale effects*. Technical Paper 82-3, U.S. Army Engineer Waterways Experiment Station, Coastal Engineering Research Center, Vicksburg, MS.

CEM (Coastal Engineering Manual) (2006 a). Part VI, Chapter 2: Types and Functions of Coastal Structures. (US Army Corps of Engineers), June.

CEM (Coastal Engineering Manual) (2006 b). Part VI, Chapter 5: Fundamentals of Design. (US Army Corps of Engineers), June.

Contente, J. (2012). *Desenvolvimento de uma Técnica Fotogramétrica, Aplicada à Evolução do Dano em Ensaios em Modelo Reduzido de Quebra-mares de Taludes*. Estágio de final de curso. Faculdade de Ciências e Tecnologia.

Ferreira, R., Costeira, J. and Santos, J.A. (2005). Stereo Reconstruction of a Submerged Scene. *Proceedings of Second Iberian Conference, ibPRIA*, Estoril, Portugal, Part I, pp 102–109.

Ferreira, R. (2006). *Reconstruction of a Submerged Model Breakwater and Interface Estimation*. Masters degree thesis. Instituto Superior Técnico, Lisbon, Portugal

Ferreira, R., Costeira, J.P., Silvestre, C., Sousa, I. and Santos, J.A. (2006). Using stereo image reconstruction to survey scale models of rubble-mound structures. *Proceedings of 1st CoastLab 2006 - International Conference on the application of physical modelling to port and coastal protection*. Porto, Portugal, pp.107–116.

Iribarren (1938). Una formula para el calculo de los diques en escollera [A formula for the calculation of rock-fill dikes]. *Revista de Obras Publicas*, Madrid, Spain. Translated by D. Heinrich, Tech. Rep. HE-116-295, Fluid Mech. Lab., Univ. of Calif., Berkeley, CA, 1948.

Lemos, R. (2010). *Verificação de fórmulas para a evolução da erosão em taludes de quebra-mares*. Masters degree thesis. Instituto Superior de Engenharia de Lisboa, Lisbon, Portugal.

Lemos, R., Santos, J. (2012). Ensaios em Modelo Reduzido de Quebra-mares de Taludes. Aplicação da Fotogrametria no Levantamento de Perfis. *Proceedings of Mefte2012 - IV Conferência Nacional em Mecânica de Fluidos, Termodinâmica e Energia*. Lisbon, Portugal.

Hough, G.; Phelp, D. (1998) Digital imaging processing techniques for the aerial field monitoring of harbour breakwaters. *Proceedings of International Conference on Coastal Engineering*, pp. 1789–1799.

Hudson, R.Y. (1958). *Design of quarry stone cover layers for rubble-mound breakwaters*. Hydraulic laboratory investigation. Research report No. 2-2, U.S. Army Engineer Waterways Experiment Station, Vicksburg, USA.

Jackson, R.A. (1968). *Design of cover layers for rubble-mound breakwaters subjected to non-breaking waves*. Research report No. 2-11, U.S. Army Engineer Waterways Experiment Station, Vicksburg, USA.

Santos, J.A; Neves, M.G.; Silva, L.G. (2003). Rubble-mound breakwater inspection in Portugal. *Proceedings of Coastal Structures '03*, pp. 249–261.

Silvestre, C.; Oliveira, P.; Pascoal, A.; Sebastião, L.; Santos, J.A.; Silva, L.G.; Neves, M.G. (2004). Inspection and diagnosis of Sines' west breakwater. *Proceedings of International Conference on Coastal Engineering*, pp. 3555–3567.

Van Der Meer, J.W. (1987) - Stability of breakwater armour layers: design formulae. *Proceedings of International Conference on Coastal Engineering*, pp. 219–239.

Van Der Meer, J.W. (1988). *Rock slopes and gravel beaches under wave attack*. Ph.D. thesis, Delft University of Technology, The Netherlands; Also Delft Hydraulics Publ. 396.

Wolters, G., Van Gent, M.R.A. (2010). Oblique wave attack on cube and rock armoured rubble mound breakwaters. *Proceedings of 32nd ICCE*, Shanghai.

Van Gent, M.R.A. (2014). Oblique wave attack on rubble mound breakwaters. *Proceedings of Coastal Engineering*, pp. 43–54.

Hofland, B., Van Gent, M.R.A., Raaijmakers, T., Liefhebber, F. (2011). Damage evaluation using the damage depth. *Proc. Coastal Structures 2011*, Yokohama.

Loop, C. and Zang, Z. (1999). Computing Rectifying Homographies for Stereo Vision. *IEEE Conf. Computer Vision and Pattern Recognition*, 1999.

Zhang, Z. (1999). *Flexible Camera Calibration by Viewing a Plane from Unknown Orientations*. Microsoft Research, 1999.

Mattoccia, S. (2015). *Stereo Vision: Algorithms and Applications*. Department of Computer Science (DISI), University of Bologna.

Lagendijk, R.L., Franich, R.E., & Hendriks, E.A. (2002). *Stereoscopic Image Processing*. Delft University of Technology, Electrical Engineering, Delft, The Netherlands.